The International Journal of Advanced Manufacturing Technology (2018) 96:3235–3249
https://doi.org/10.1007/s00170-018-1819-y

ORIGINAL ARTICLE

Dynamic digital fringe projection technique for measuring the warpage of unpainted PBGA packages and boards

Sungbum Kang [1] · I. Charles Ume [2]

Received: 1 November 2017 / Accepted: 18 February 2018 / Published online: 2 March 2018

Abstract
A crucial factor for ensuring the reliability of chip packages is the measurement and control of warpage. The warpage of chip packages, printed wiring boards (PWBs), and PWB assemblies (PWBAs) are typically measured by moiré techniques (i.e., shadow moiré, laser fringe projection, and digital fringe projection), which have noncontact, full-field, and high-resolution capabilities. The application of moiré techniques typically involves spraying a mist of reflective paint on the surface of a sample to ensure the uniformity of surface reflectance and to obtain better fringe image contrast and better sinusoidal waveforms in the fringe patterns for the measurement process. However, since painted samples may no longer be re-used, the process of spray painting is not suited for inline inspection; a new technique for measuring warpage without painting is required. In this research, a dynamic digital fringe projection (DDFP) technique for measuring the warpage of unpainted plastic ball grid array (PBGA) packages and boards was developed. The DDFP technique dynamically determines proper fringe intensity distributions for PBGA packages and PWBs and uses them to produce a better fringe image contrast and better sinusoidal waveforms without painting. Experimental results showed that the DDFP technique successfully measures the warpage of PBGA packages and PWBs in unpainted PWBAs accurately.

Keywords Warpage · Electronic packaging · Digital fringe projection · Dynamic digital fringe projection

1 Introduction

Over the years, integrated circuit technologies have become increasingly sophisticated and now consist of smaller chip sizes and higher density circuitry while satisfying superior reliability requirements. This trend, however, has been accompanied by the issue of warpage, which occurs primarily during the reflow process when chip packages are soldered to printed wiring boards (PWBs) in a reflow oven and later cooled down to room temperature as the assembled boards exit the oven. Warpage is induced by coefficient of thermal expansion (CTE) mismatches between various materials within chip packages and PWBs. If induced warpage in chip packages or PWBs are larger than their critical values, they can cause component misregistration during the component placement and insertion processes. The presence of warpage can also cause reliability problems in chip packages such as die cracking, underfill delamination, and fatigue failure in solder bumps resulting from high residual stresses [1, 2], as illustrated in Fig. 1.

The influence of warpage on the failure of chip packages has made warpage control a critical factor during the reflow process. To address this concern, the first step is to measure the warpage accurately and quickly. Several techniques for measuring the warpage of chip packages and boards (i.e., PWBs and PWB assemblies) have been developed. In the early days, contact measurement techniques, such as the contact profilometer, were used to measure warpage. As the measurement requirement calls for higher throughput and in-line measurement capabilities, several noncontact warpage measurement techniques were developed.

For example, moiré techniques are widely used to measure the warpage of chip packages and boards due to their noncontact, full-field, and high-resolution measurement capabilities. The moiré techniques use fringe patterns to obtain the out-of-plane displacement of a sample surface, and they can be

✉ I. Charles Ume
charles.ume@me.gatech.edu

[1] Technology & Manufacturing Group, Intel Corporation, Hillsboro, OR 97124, USA

[2] School of Mechanical Engineering, Georgia Institute of Technology, Atlanta, GA 30332, USA

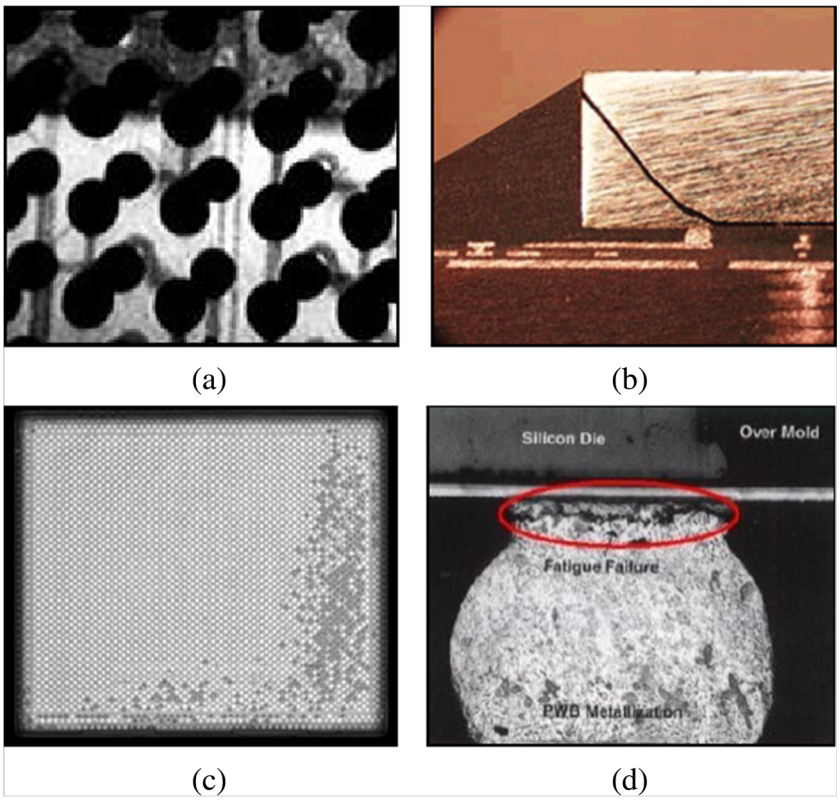

Fig. 1 **a** Component misregistration. **b** Die cracking. **c** Underfill delamination. **d** Solder bump fatigue failure [2]

classified into the following three types based on how they generate the fringe patterns: the shadow moiré, laser fringe projection (LFP), and digital fringe projection (DFP) techniques. The shadow moiré uses glass grating, located very close to the sample, to generate the fringe patterns. This technique is the most commonly used for measuring warpage because it is easy to set up and calibrate, and it is fast and therefore facilitates image calculations [3]. However, it is not a suitable technique for simultaneously measuring the warpage of chip package(s) and PWB in a PWB assembly (PWBA) because the glass grating must be placed very close to the sample surface [3]. Such proximity can also affect the thermal behavior of the sample during the reflow process [3].

The fringe projection techniques (i.e., the LFP and DFP techniques) can be used to overcome these disadvantages of the shadow moiré technique because they do not require glass grating. Instead, the LFP technique typically uses a laser interferometer to generate the fringe patterns. Its major disadvantage, however, is its noisy fringe patterns caused by laser speckle [4]. The DFP technique overcomes this drawback because it uses a digital projector to generate the fringe patterns. However, the DFP technique has its own disadvantage in the form of gamma nonlinearity [5], which represents the nonlinear relationship between the input and output intensities of the digital projector.

Chang et al. [6] applied a digital light processing (DLP) projector and a set of optical lenses to a DFP system for measuring the warpage of a flip-chip ball grid array (BGA) package and the profile of a solder ball of a flip chip package. They reduced the fringe pitch by directing the fringe pattern into a stereo zoom microscope. Yen et al. [7, 8] also used a DFP system with a DLP projector for measuring the coplanarity of solder balls of BGA packages. Joo and Kim [9] enhanced the sensitivity of a DFP system by using immersion interferometry and the optical/digital fringe multiplication method that enables a 52-nm fringe pitch. Pan et al. [10] measured the warpage of plastic ball grid array (PBGA) packages using a DFP system with a resolution of 3 μm. Pan et al. [10] also developed a microscopic DFP system to measure the warpage of chip packages with size below 10 × 10 mm. The system enables fringe pitch of 80 μm. Shien et al. [11] developed a novel measurement system utilizing the DFP technique and measured the warpage of BGA packages. The results showed that the accuracy is 2.6 μm [11]. Michael et al. [12] used a fringe projection system to measure a PWBA during the reflow process with resolution of 2.5 μm.

The moiré techniques are phase-based method like Fourier transformation [13] and fringe center [14] methods, which analyze the phase distribution of the fringe patterns reflected from a sample surface and modulated by its height distribution. Low fringe image contrast and nonideal sinusoidal waveforms in the fringe patterns cause errors in the modulated phase distribution that decrease the measurement accuracy [5].

To reduce these error sources, the use of the moiré techniques in the measurement process generally requires spraying the sample surface with a mist of reflective paint in order to ensure uniform surface reflectance and better fringe image contrast. Painted samples, however, may not be reused, and the spray-painting process is not suitable for use in the assembly line. When an unpainted PWBA containing a PBGA package is measured using the DFP technique, variances in surface reflectance between the PBGA package and the PWB generally result in either too dark or too bright regions in the PWBA fringe image. For example, when a dark fringe pattern (Fig. 2a) is projected onto the PWBA, the PWB region of the PWBA fringe image (Fig. 2b) is too dark for processing. In contrast, when a bright and uniform fringe pattern (Fig. 2c) is projected onto the PWBA, the package region of the PWBA fringe image (Fig. 2d) is too bright for processing. This problem can be solved by projecting a fringe pattern containing varying intensities, shown in Fig. 2e, in order to obtain a fringe image with improved fringe image contrast as shown in Fig. 2f.

In order to accurately measure the warpage of PBGA packages and boards in a PWB assembly without painting them with a mist of reflective paint, a dynamic digital fringe projection (DDFP) technique was developed. The DDFP technique generates and projects a dynamic fringe pattern, in which proper fringe intensity distributions are dynamically determined based on the coordinates and the surface reflectance of PBGA packages and PWBs. It increases fringe image

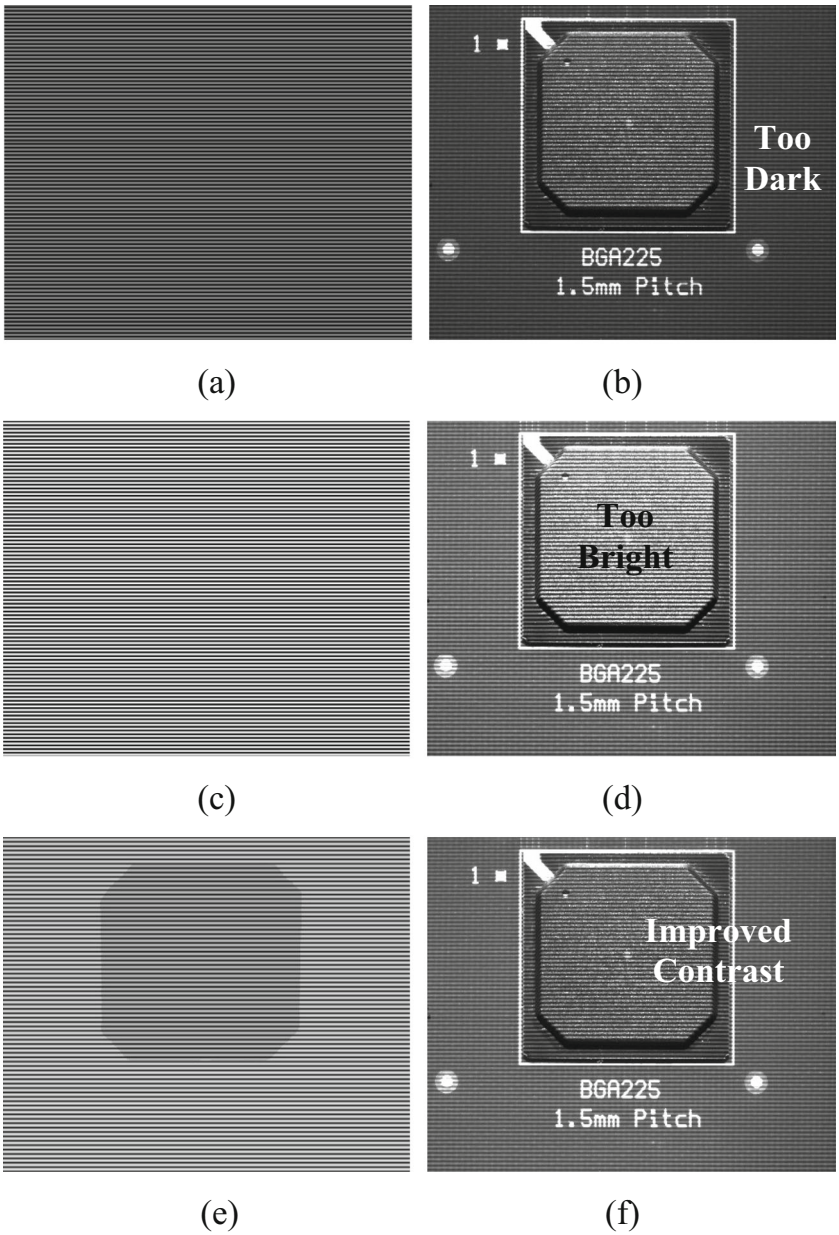

Fig. 2 **a** A dark fringe pattern. **b** A PWBA fringe image illuminated by **a**. **c** A bright fringe pattern. **d** A PWBA fringe image illuminated by **c**. **e** A dynamic fringe pattern. **f** A PWBA fringe image illuminated by (**e**)

contrasts and reduces nonideal sinusoidal waveforms in the fringe patterns when measuring unpainted PWB assemblies.

2 Dynamic digital fringe projection technique

DDFP technique incorporates the DFP technique's measurement processes [15] for measuring the warpage of painted chip packages and boards. The steps of the process are (1) to generate and project a sinusoidal fringe pattern onto a sample surface [16], (2) to obtain four-step phase-shifted fringe images reflected from the sample surface [17], (3) to apply the four-step phase-shifting method to the captured fringe images to obtain a wrapped phase image [17], (4) to apply the mask-cut phase unwrapping algorithm to the wrapped phase images to obtain an unwrapped phase image [18, 19], (5) to convert the unwrapped phase image to a displacement image that contains the surface height distribution using the reference-subtraction and the linear conversion methods [5, 20], and (6) to obtain the warpage of the sample from the displacement image [15]. Here, four-step phase shifting method was used to increase the measurement resolution. Four-step phase was chosen because the measurement resolution is not significantly different for the phase-shifting method that uses more than four steps [21].

In addition to incorporating the DFP technique's measurement processes, the DDFP technique includes an automatic method for segmenting the PBGA package and PWB regions in an unpainted PWBA image, together with calibration methods to compensate for the mismatches in coordinates and intensities between the projected and captured images. Because coordinate calibration is independent of sample changes, it needs to be performed only once after the system is set up. After the segmentation and the calibrations are performed, the DDFP technique generates a dynamic fringe pattern and projects it onto the unpainted PWBA. Figures 3 and 4 present the flowchart and sample images depicting the process of the DDFP technique, and the remainder of this chapter details the first four steps of the process, which differ from those of the DFP technique.

2.1 Coordinate calibration between projected and captured images

The coordinates of projected and captured images differ; that is, the fields of view of the projector and the camera do not perfectly match, causing misalignment of the projected dynamic fringe pattern, shown in Fig. 5c.

To calibrate the coordinate mismatches, coordinate transfer functions (CTFs) were obtained using a checkered pattern [22] and projector-camera homography [23]. A checkered pattern with $n \times m$ squares was generated, projected, and captured, which, in turn, divided the projected and captured images into $n \times m$ divisions, shown in Fig. 6.

The CTF for the ith division is provided in Eq. 1 [23], in which $T_{i,j}$ is calculated by the eigenvector corresponding to the smallest eigenvalue of $A^{\mathrm{T}}A$, where A is given in Eq. 2 [23].

$$X_i(x_i, y_i) = \frac{T_{i1}x_i + T_{i2}y_i + T_{i3}}{T_{i7}x_i + T_{i8}y_i + T_{i9}}$$
$$Y_i(x_i, y_i) = \frac{T_{i4}x_i + T_{i5}y_i + T_{i6}}{T_{i7}x_i + T_{i8}y_i + T_{i9}} \quad (1)$$

Fig. 3 Flowchart of the implementation process of the DDFP technique

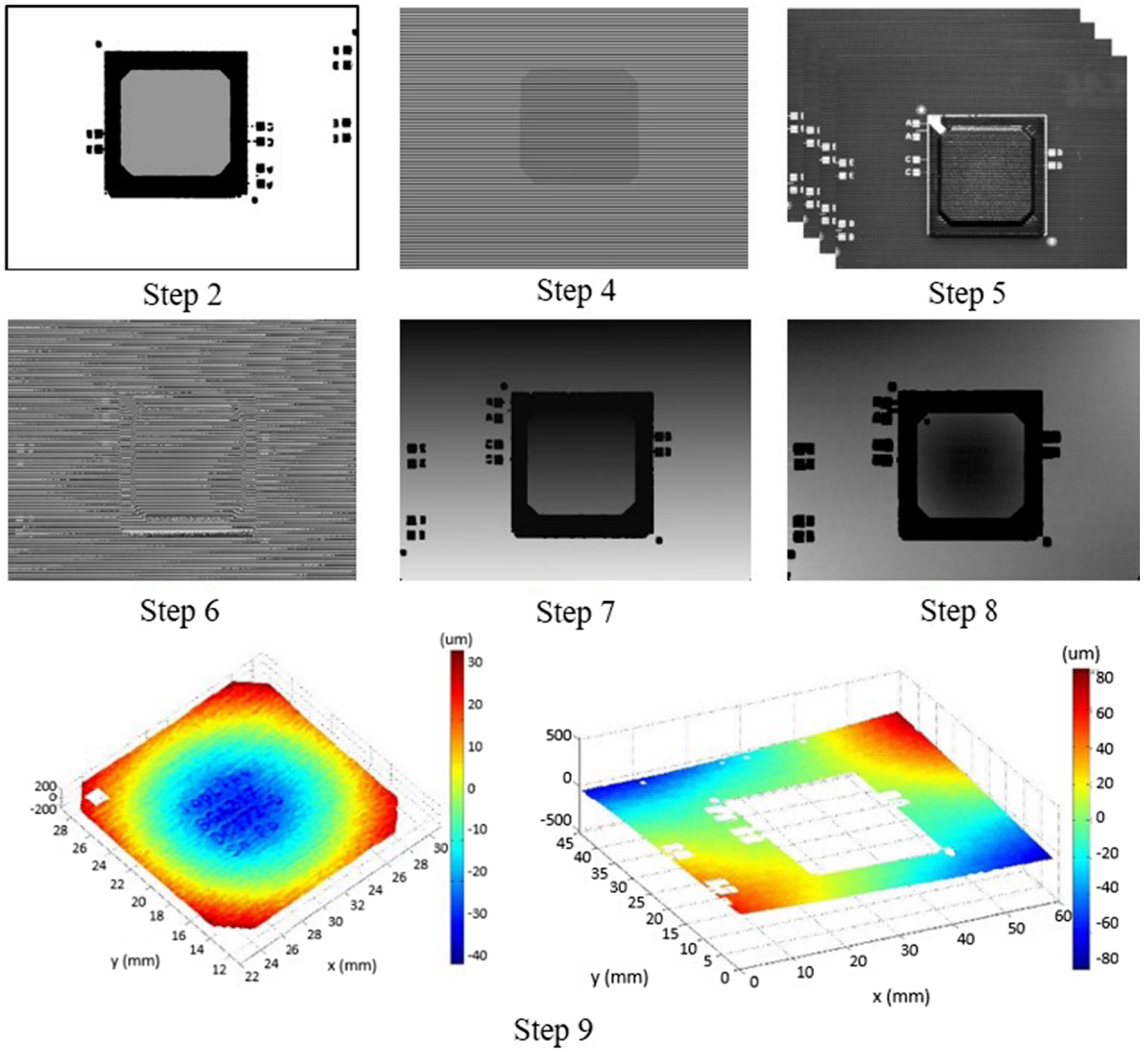

Fig. 4 Sample images obtained in each step described in Fig. 3

where (X_i,Y_i) = coordinates in the ith division of the projected image, (x_i,y_i) = coordinates in the ith division of the captured image, and $T_{i,j}$ = transformation coefficients for the ith division.

$$A = \begin{pmatrix} x_{i1} & y_{i1} & 1 & 0 & 0 & 0 & -X_{i1}x_{i1} & -Y_{i1}x_{i1} & -X_{i1} \\ 0 & 0 & 0 & x_{i1} & y_{i1} & 1 & -X_{i1}y_{i1} & -Y_{i1}y_{i1} & -Y_{i1} \\ \vdots & \vdots & \vdots & \vdots & \vdots & \vdots & \vdots & \vdots & \vdots \\ x_{i4} & y_{i4} & 1 & 0 & 0 & 0 & -X_{i4}x_{i4} & -Y_{i4}y_{i4} & -X_{i4} \\ 0 & 0 & 0 & x_4 & y_4 & 1 & -X_{i4}y_{i4} & -Y_{i4}y_{i4} & -Y_{i4} \end{pmatrix} \quad (2)$$

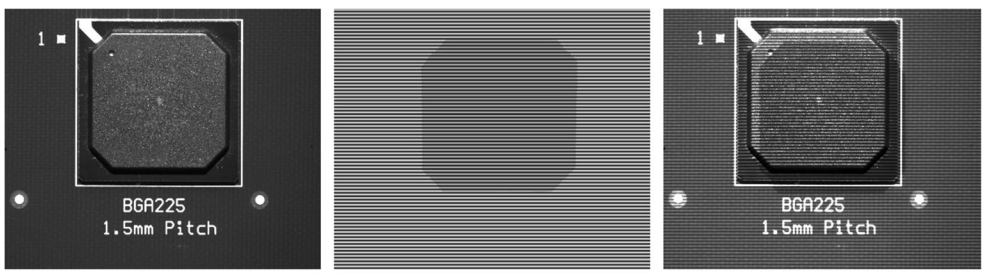

Fig. 5 **a** A PWBA image. **b** A dynamic fringe pattern generated based on the chip package coordinates in **a** (for example, the fringe intensities in the PBGA package region are darker than those in the PWBA region and the intensities of each region are determined by the intensity calibration introduced in Sect. 2.3). **c** A PWBA fringe image illuminated by **b**

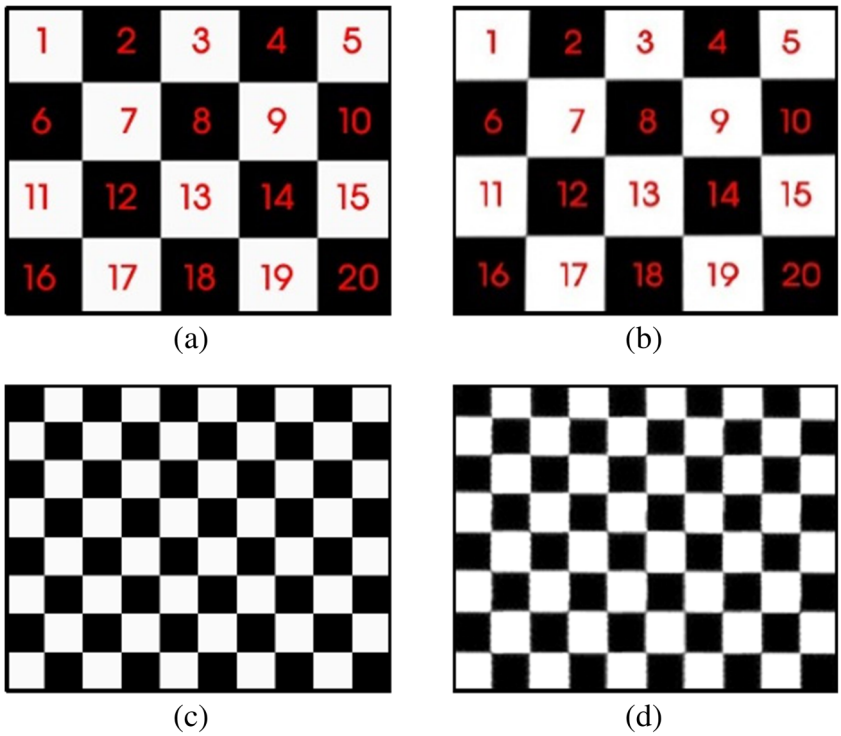

Fig. 6 Square divisions in the **a** projected and **b** captured images when a 5 × 4 checkered pattern is used and square divisions in the **c** projected and **d** captured images when a 10 × 8 checkered pattern is used

where (X_{i1}, Y_{i1})~(X_{i4}, Y_{i4}) = the four corner coordinates of the *i*th division in the projected image and (x_{i1}, y_{i1})~(x_{i4}, y_{i4}) = the four corner coordinates of the *i*th division in the captured image.

The CTFs are used to modify the coordinates in the projected image in order to compensate for the coordinate mismatches between the projected and captured images. To validate the coordinate calibration, the coordinates of 35 equally distributed cross marks between the projected and captured images were compared before and after the coordinate calibration. Coordinate transfer errors were quantified by the average differences between the mark coordinates for the projected and captured images. Because the number of the squares ($n \times m$) in the checkered pattern affects the quantity of coordinate transfer errors [24], the coordinate transfer errors were obtained with various numbers of squares, as shown in Fig. 7. Here, the errors before the calibration are reflected when n is zero. As the figure shows, the coordinate transfer error decreases when n increases up to 25. Therefore, a 25 × 18 checkered pattern was used to calibrate the coordinates (m is 18 when n is 25).

2.2 Segmentation of the PBGA package and PWB regions in unpainted PWBA images

To generate dynamic digital fringes and measure the warpage of PBGA package(s) and PWB in an unpainted PWBA, the PBGA package and PWB regions in an unpainted PWBA image are segmented using the RGM [25]. The process of the RGM consists of the following steps: (1) capturing an unpainted PWBA image, (2) smoothing the PWBA image using the Gaussian filter [26], (3) generating the edges around each smoothened feature using the Canny algorithm [27], (4) segmenting the regions in the edged image with labels using the region-growing algorithm [28], and (5) detecting the

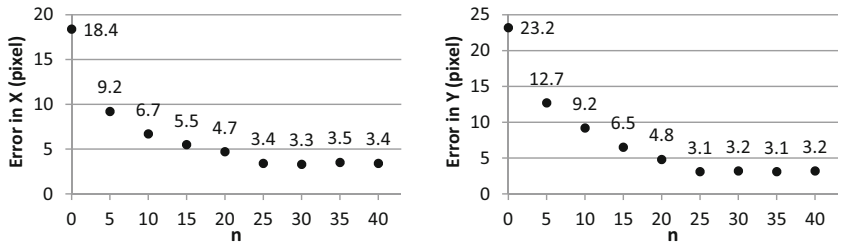

Fig. 7 Coordinate transfer errors when n of the checker pattern increases

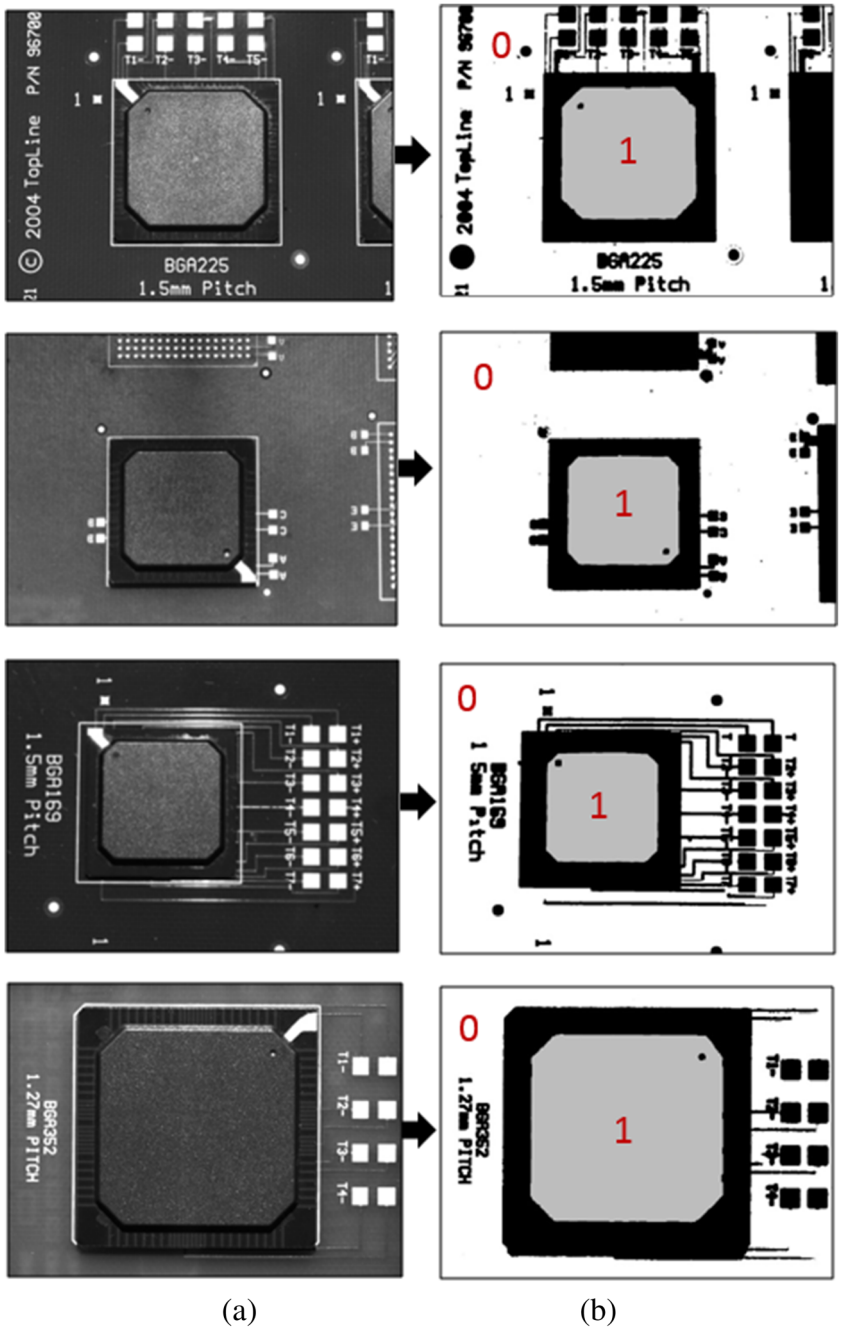

Fig. 8 **a** Unpainted PWBA images and **b** resulting segmentation images [25]

PBGA package and PWB regions in the label image using geometric analysis [25]. The RGM was designed for PWBAs that contain PBGA package(s) larger than 14×14 mm [25]. For the details of each step of the RGM, refer to [25]. Samples of the unpainted PWBA images and the resulting segmentation images produced by the RGM are shown in Figs. 8 and 9. The detected PWB and PBGA regions are marked with "0" and "1," respectively. As shown in those figures, when we use the RGM, the substrate regions and surface patterns such as copper patterns and inscriptions are masked-out (in black).

2.3 Intensity calibration between projected and captured images

Figure 10 shows the intensity flow in the DFP system. The intensity transfer function (ITF) represents the relationship between computer input intensity (I_I) and captured intensity (I_C). This relationship is generally nonlinear due primarily to the gamma nonlinearity of the digital projector [29]. The nonlinearity between I_I and I_C causes the presence of nonideal sinusoidal waveforms in the captured fringe images, which decreases the measurement accuracy and repeatability of the DFP system

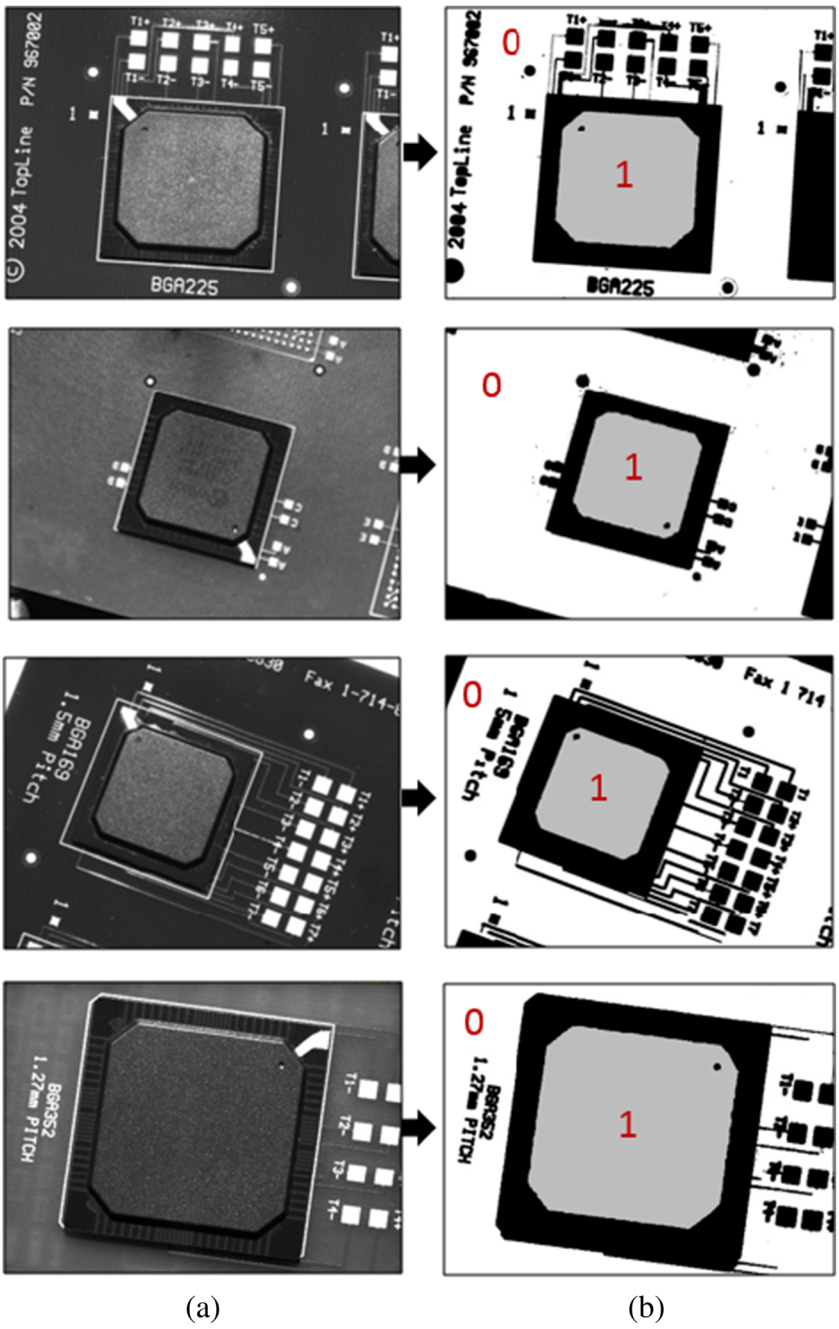

Fig. 9 **a** Unpainted PWBA images (rotated) and **b** resulting segmentation images [25]

[5]. Figure 11 illustrates this nonlinearity for the PBGA surface of a PWBA. In this case, the average absolute error between I_I and I_C is 19.1.

To calibrate the nonlinearity for unpainted samples, the polynomial regression method [29, 30] is applied together with the lookup table method [30]. A third-order polynomial regression equations (or ITF) between I_I and I_C for each of the PBGA and PWB surfaces of an unpainted PWBA are obtained by regressing six measured intensities for each surface. Figure 12 shows the ITF obtained using the polynomial regression method for an unpainted PBGA surface.

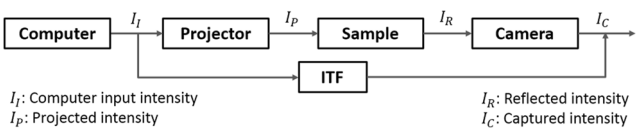

Fig. 10 Intensity flow in the DFP system

Using the ITF, a lookup table of the sample surface is created, which stores 255 I_C values and corresponding I_I values. Ultimately, the lookup table is used to calibrate input intensity in order to compensate for the nonlinearity [30]. As shown in Fig. 13, the nonlinearity significantly declines after

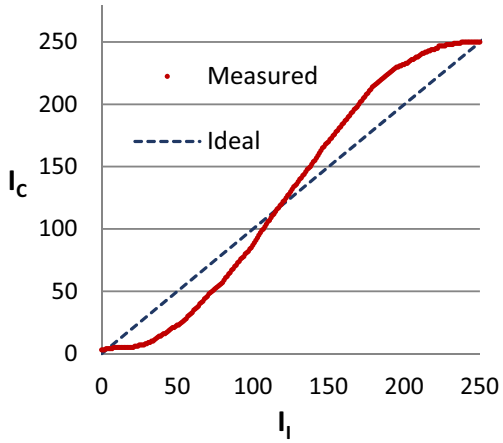

Fig. 11 Relationship between I_I and I_C for an unpainted PBGA surface

the calibration. In this case, the average absolute error between I_I and I_C is 4.1. When measuring a PWBA, intensities are simultaneously calibrated for each of the PBGA package and PWB surfaces.

2.4 Generation and projection of a dynamic fringe pattern

After the coordinate and intensity calibrations, a dynamic fringe pattern is generated. The coordinates of the PBGA package region in the segmented label image (Fig. 14a) are converted to those coordinates in the dynamic fringe pattern (Fig. 14b). For each region in the segmented label image, separate lookup table obtained from the intensity calibration that is used to produce a proper fringe intensity distribution is determined, as depicted in Fig. 14b. After the dynamic fringe pattern is generated, it is projected onto the PWBA, as shown in Fig. 14c.

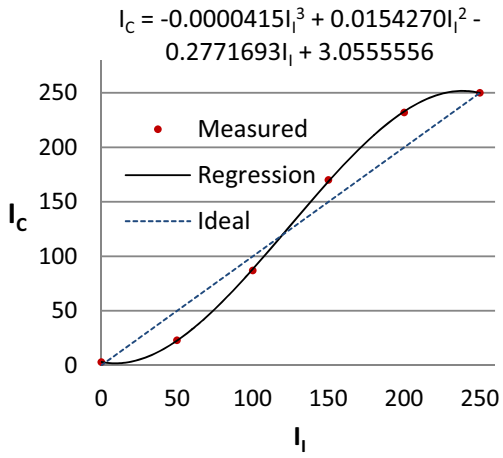

Fig. 12 An ITF obtained by regressing six measured intensities reflected from an unpainted PBGA surface

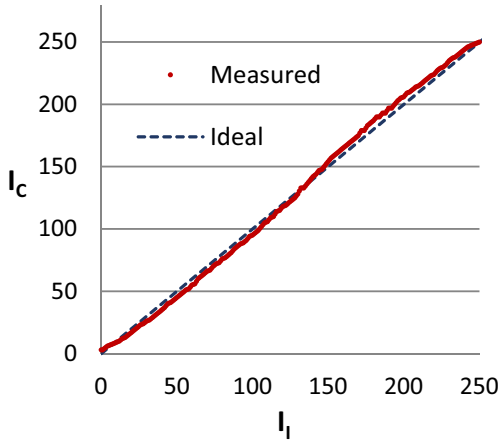

Fig. 13 Relationship between I_I and I_C after the intensity calibration for an unpainted PBGA surface

3 Experimental system

The setup of the DFP system developed in this study is illustrated in Fig. 15, which consists of a charge-coupled device (CCD) camera and a digital light processing (DLP) projector. The resolution and the frame rate of the camera are 1280 × 960 pixels and 32 frames/s, respectively, and those of the projector are 1280 × 800 pixels and 60 frames/s. The DDFP measurement technique is a modified version of the DFP system. A dynamic fringe pattern is generated by a computer and projected through a digital projector onto the sample surface. The image of the projected fringe pattern in its 60 × 45 mm field of view (FOV) is captured by a CCD camera, which results in 46.89 μm/pixel of image resolution in the *xy* plane. The theoretical out-of-plane resolution of the DFP system can be calculated using Eq. 3 [10]. For the calculation, the values of P, α, β, and C of the DFP system are 0.6 mm in the x-direction, 0°, 45°, and 256, respectively. The theoretical resolution of the DFP system is 2.34 μm in the z-direction.

$$R = \frac{P}{C(\tan\alpha + \tan\beta)} \tag{3}$$

where R = resolution, P = fringe pitch, α = observation angle, β = illumination (or projection) angle, and C = coefficient of resolving power for the gray level of the light intensity.

The DFP system includes customized software written in the C++ programming language. All the processing algorithms, such as the phase wrapping and unwrapping algorithms, are implemented in the software. The same software controls the camera which captures the images, and the projector which projects and shifts the fringe patterns. The user interface of the software is shown in Fig. 16. All the algorithms and functions embedded in the software are automated so that it can run without operator interference.

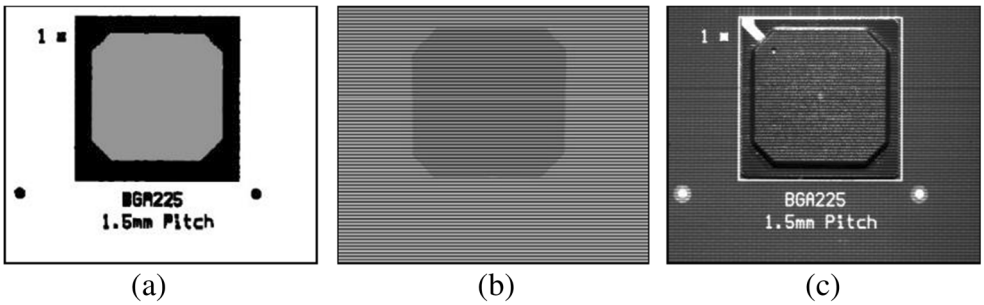

Fig. 14 **a** The segmented label image, **b** the dynamic fringe pattern, and **c** the PWBA fringe image illuminated by **b**

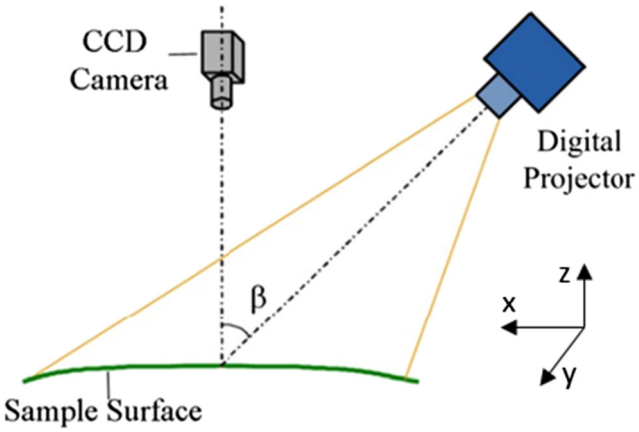

Fig. 15 Setup of the DFP system

A calibration block with five steps (6, 14, 39, 87, and 163 μm) was used to validate the DFP system developed in this study. Using the DFP system, each step of the calibration block was measured ten times. The averages ($\bar{y}$), the percentage errors (Ɛ), and the standard deviations (σ) [31] of the ten measurements are summarized in Table 1. From those results, the measurement accuracy and repeatability were quantified as 1.07 and 0.52 μm, respectively, by the mean absolute error [31] and the pooled standard deviation [32]. It shows that the system has very high accuracy and repeatability considering the resolution of the system that is 2.34 μm.

4 Results and discussions

To validate the DDFP technique, four PBGA packages and two PWBs, shown in Fig. 17, were used. The sizes of the three-layer

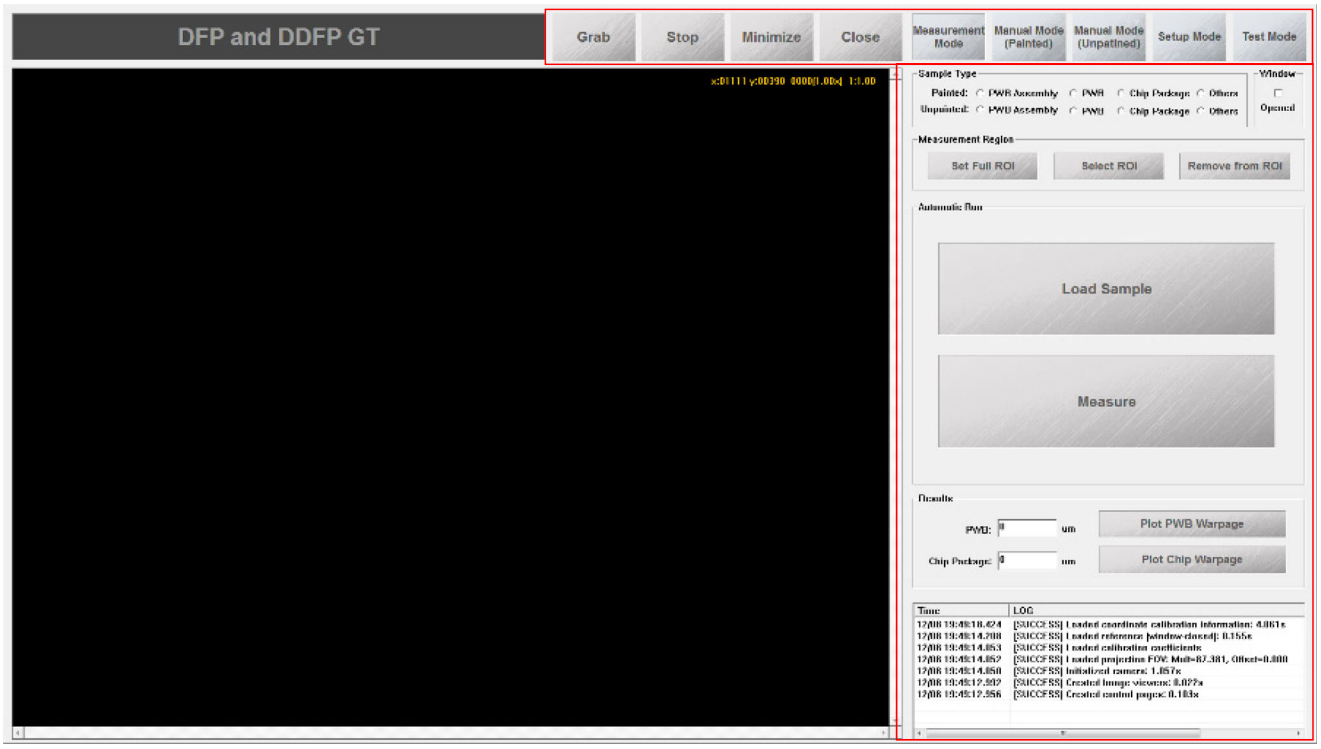

Fig. 16 The user interface of the customized software

Table 1 The results of the calibration block measurements

Step height (μm)	6	14	39	87	163
$\bar{y}$ (μm)	6.45	14.84	37.65	85.18	162.12
(μm)	0.45	0.84	− 1.35	− 1.82	− 0.88
σ (μm)	0.37	0.40	0.59	0.69	0.50

PWBs are 200 × 140 mm and the thicknesses are 1.5 mm. The sizes of the PBGA packages are 23 × 23 mm, 27 × 27 mm, 35 × 35 mm, and 27 × 27 mm, and the substrate materials of the PBGA packages are bismaleimide-triazine. The heights of the PBGA packages used in this study are 1.53 mm, and the heights of commercially available PBGA packages are from

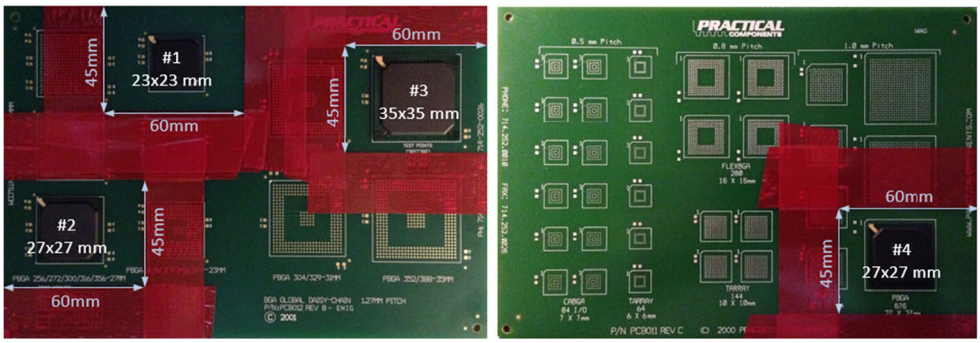

Fig. 17 **a** PWBA1 with three PBGA packages and **b** PWBA2 with one PBGA package

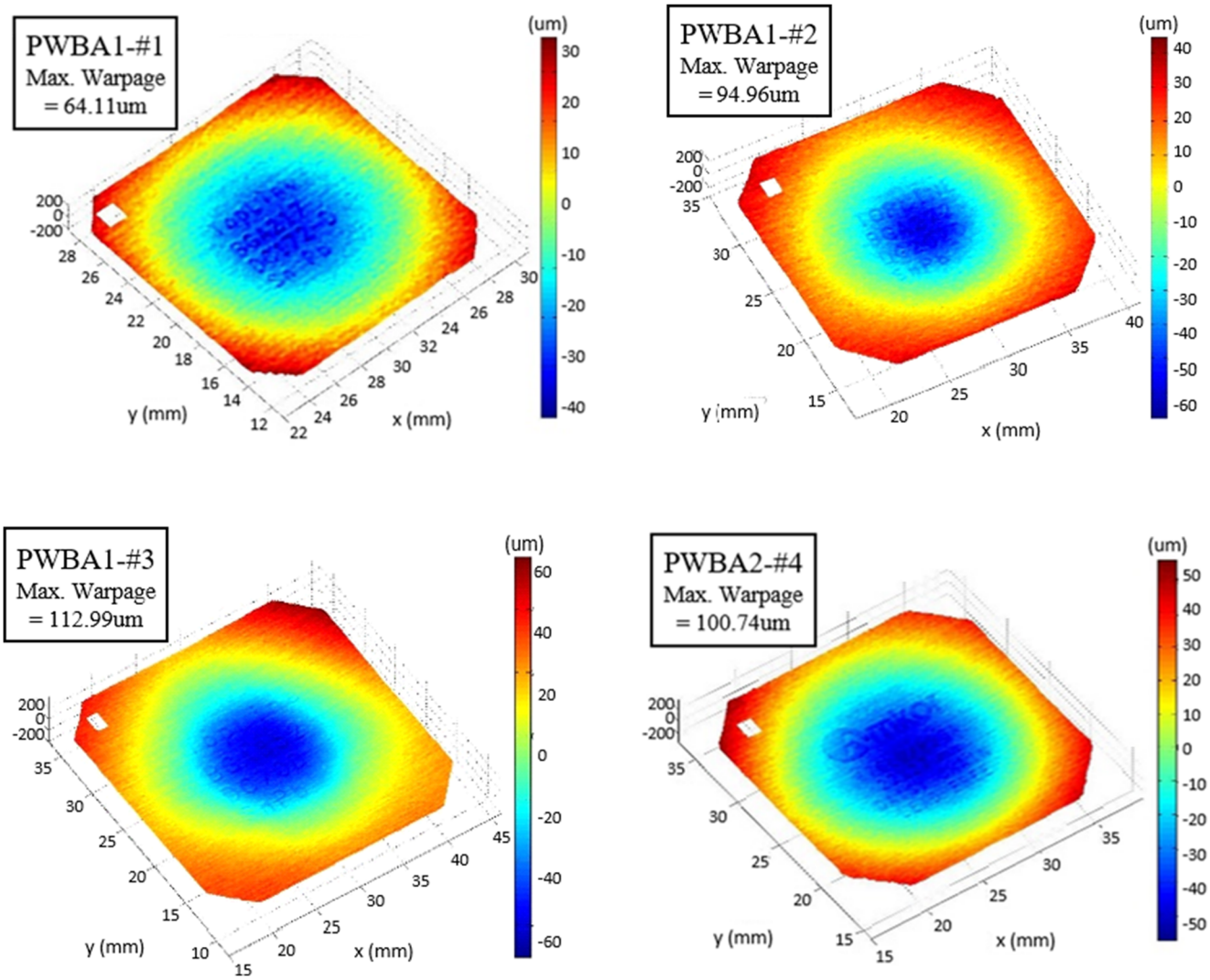

Fig. 18 Warpage of PBGA packages obtained with the DDFP

1.4 to 2.33 mm. The package height does not affect the measurement because the system covers up to 16.2 mm.

The four PBGA packages and two PWBs were reflowed separately in a reflow oven that uses the typical ramp to dwell and ramp to peak temperature profile [2] to generate the warpage of each of them. The warpage of the four PBGA packages and four PWB regions (60 × 45 mm) shown in Fig. 16 was separately measured using a contact profilometer with a resolution of less than 0.1 μm as a reference. Red masking tapes were placed on the PWBs to ensure consistency of the fields of view in all measurements. Using an adhesive, PBGA packages were temporarily attached to the PWBs in order to simulate PWBAs. Then, using the DDFP system, the warpage of the PBGA package and the PWB in each of the four PWBA regions (60 × 45 mm) were simultaneously measured as shown in Figs. 18 and 19.

Next, the PBGA packages were detached from the PWBs. Both the PBGA packages and the PWBs (60 × 45 mm) were sprayed with thin film of white paint, and their warpage was separately measured using the shadow moiré system as shown in Figs. 20 and 21. The shadow moiré system uses four-step phase shifting method.

The measurement results are summarized in Tables 2 and 3. The contact profilometer results were used as references and were used to compare the DDFP and shadow moiré results. These comparisons show that the absolute measurement errors of the DDFP results were less than 8% while the absolute measurement errors of the shadow moiré results were less than 5%. The major advantage of the DDFP technique is that it can be used to simultaneously measure the warpage of PBGA packages and PWB in a PWBA without spraying it with a thin film of paint. Therefore, the DDFP technique is the only warpage measurement technique that can be used in the assembly line during the PWB assembly process to measure warpage of the PBGA and PWB. On the other hand, if the PWB surface has too many surface patterns such as copper patterns and inscriptions, the DDFP technique can be less accurate because it masks out these patterns during measurement as shown in Fig. 18. If the masked out regions include the highest and/or the lowest points of the warped PWB surface, they will not be captured by this method.

5 Conclusion

This work introduced a novel technique, dynamic digital fringe projection (DDFP), the first of its kind, for measuring

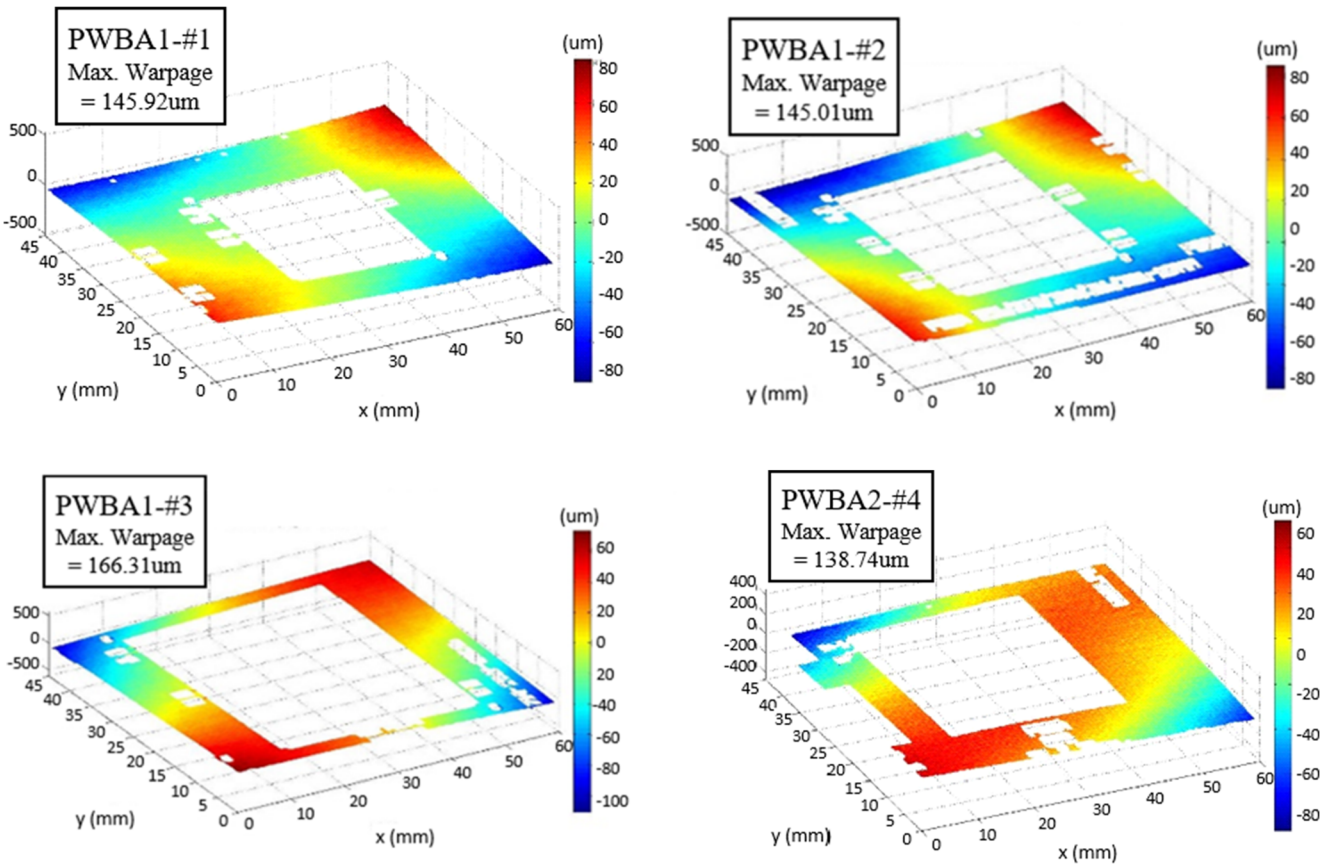

Fig. 19 Warpage of PWBs obtained with the DDFP

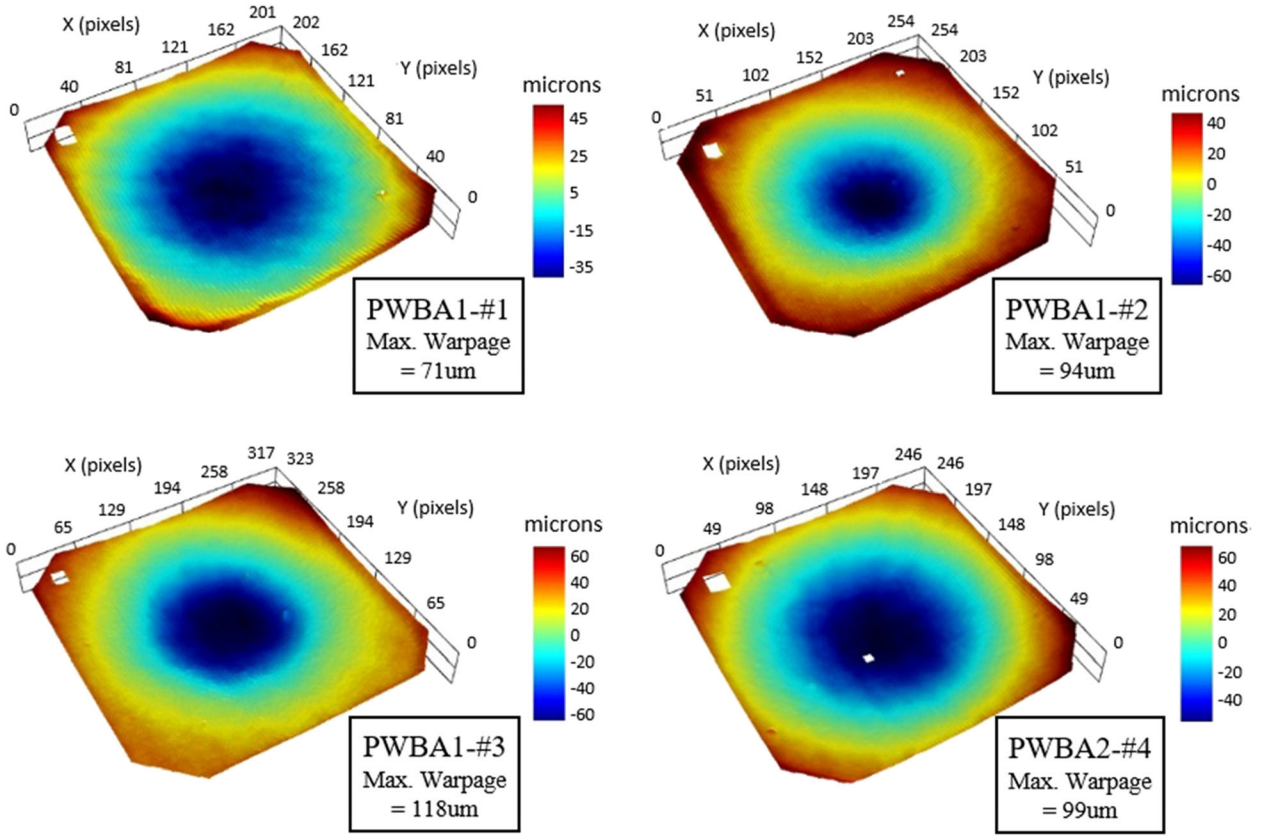

Fig. 20 Warpage of PBGA packages obtained with the shadow moiré

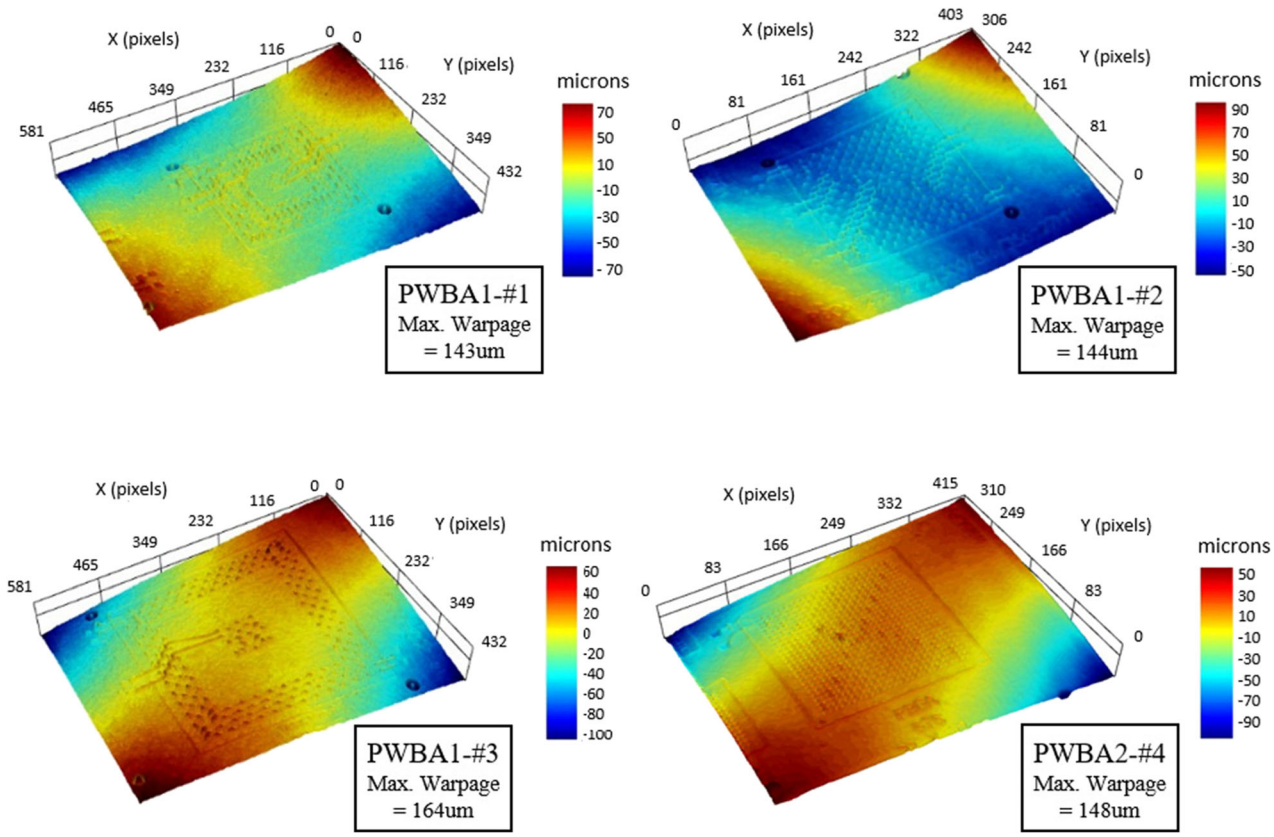

Fig. 21 Warpage of PWBs obtained the shadow moiré

Table 2 Comparison of the warpage of PBGA packages measured with the contact profilometer (CP), shadow moiré (SM), and DDFP

Sample	Max. warpage (μm)			% Error	
	CP[a]	SM[b]	DDFP[c]	SM (%)	DDFP (%)
PWBA1-no. 1	67.80	70.33	64.40	3.74	5.01
PWBA1-no. 2	90.33	93.67	95.02	3.69	5.19
PWBA1-no. 3	120.21	118.33	113.48	1.56	5.60
PWBA2-no. 4	94.51	98.67	100.53	4.40	6.36

[a] Used as reference (CP resolution < 0.1 μm)

[b] Average of three measurements (SM resolution = 0.83 μm when using 300 lines/in. grating)

[c] Average of ten measurements

the warpage of unpainted plastic ball grid array (PBGA) package(s) and printed wiring board (PWB) in a PWB assembly. The DDFP technique includes a method for segmenting the PBGA package and PWB regions in an unpainted PWB assembly image. It also includes calibration methods for compensating the coordinate and intensity mismatches between projected and captured images. Experimental results showed that the DDFP technique successfully measured the warpage of PBGA packages and PWBs in unpainted PWBAs. When compared to the contact profilometer, DDFP produced a measurement error of less than 8%. Even though this study demonstrated how to use the DDFP technique to measure the warpage of PBGA and PWBs in PWB assemblies, further research can be conducted to demonstrate how to extend this technique to measure the warpage of other chip packages. Because of rapid advances in digital technologies, this new technique can potentially be used for making accurate measurements of the warpage of unpainted PBGA packages and PWBs in an assembly line when chip packages such as PBGAs are being assembled on a PWB.

Table 3 Comparison of the warpage of PWBs measured with the contact profilometer (CP), shadow moiré (SM), and DDFP

Sample	Max. warpage (μm)			% Error	
	CP[a]	SM[b]	DDFP[c]	SM	DDFP
PWBA1-no. 1	138.82	143.33	145.47	3.25%	4.79%
PWBA1-no. 2	136.48	142.67	146.87	4.53%	7.61%
PWBA1-no. 3	160.32	164.00	167.01	2.30%	4.17%
PWBA2-no. 4	150.18	147.67	138.45	1.67%	7.81%

[a] Used as reference (CP resolution < 0.1 μm)

[b] Average of three measurements (SM resolution = 0.83 μm when using 300 lines/in. grating)

[c] Average of ten measurements

References

1. Tummala R, Rymaszewski EJ, Klopfenstein AG (2001) Microelectronics packaging fundamentals. McGraw-Hill, New York
2. Tan W (2008) Development of convective reflow-projection moire warpage measurement system and prediction of solder bump reliability on board assemblies affected by warpage, Mech Eng. Georgia Institute of Technology, Atlanta, GA. http://hdl.handle.net/1853/22600
3. Ding H, Powell RE, Hanna CR, Ume IC (2002) Warpage measurement comparison using shadow Moire and projection Moire methods. IEEE Trans Comp Packag Technol 25:714–721
4. Kang S, Gong J, Ume IC (2011) Determination of Optimum Values of Control Parameters to Reduce Laser Speckle Noise for Projection Moiré System, ASME ASME International Mechanical Engineering Congress and Exposition 1:743–749. https://doi.org/10.1115/IMECE2011-62766
5. Gorthi SS, Rastogi P (2010) Fringe projection techniques: whither we are? Opt Lasers Eng 48:133–140
6. Chang C-S, Shao C-A, Wu E (2004) Micro-scaled surface profile measurement on packages by digital projection moiré. ASME Electron Photon Packag 4:161–166
7. Yen H-N, Tsai D-M, Yang J-Y (2006) Full-field 3-D measurement of solder pastes using LCD-based phase shifting techniques. IEEE Trans Electron Packag Manuf 29:50–57
8. Yen H-N, Tsai D-M, Feng S-K (2008) Full-field 3-D flip-chip solder bumps measurement using DLP-based phase shifting technique. IEEE Trans Adv Packag 31:830–840
9. Joo J-W, Kim H-J (2008) Nano-level high sensitivity measurement using microscopic Moiré interferometry. Transactions of the Korean Society of Mechanical Engineers—A 32:186–193
10. Pan J, Zwemer DA, Petriccione G, and Curry R (2006) Thermally-induced warpage measurement on small packages by a microscopic fringe projection system, Thermal and Thermomechanical Proceedings 10th Intersociety Conference on Phenomena in Electronics Systems, San Diego, CA, pp. 953–960. https://doi.org/10.1109/ITHERM.2006.1645449
11. Ri S, Muramatsu T, Saka M, Tanaka H (2012) Fast and accurate shape measurement system utilizing the fringe projection method with a ferroelectric liquid-crystal-on-silicon microdisplay. Opt Eng 51:081506–081501
12. Hertl M, Weidmann D (2011) Innovative assessment of thermomechanical stress effects in electronics components and assemblies. Electron Devic Fail Anal 13:4–11
13. Liu XFHZW, Xie HM, Lou XH, Du H (2011) The artificial periodic lattice phase analysis method applied to deformation evaluation of TiNi shape memory alloy in micro scale. Meas Sci Technol 22:125702
14. Liu Z, Huang X, Xie H (2013) A novel orthogonal transmission-virtual grating method and its applications in measuring micro 3-D shape of deformed liquid surface. Opt Lasers Eng 51:167–171
15. Kang S, Ume IC (2014) Comparison of warpage measurement capabilities and results obtained by using laser and digital fringe projection methods. J Electron Packag 136:031007–031007
16. Zhang S (2006) High-resolution, real-time 3-D shape measurement, Ph.D. Dissertation, Dept. of Mechanical Engineering, Stony Brook University, Stony Brook, NY. http://eds.a.ebscohost.com/eds/detail/detail?vid=0&sid=a099198c-b526-4492-a6c0-f8cbb2f805ad%40sessionmgr4008&bdata=JnNpdGU9ZWRzLWxpdmUmc2NvcGU9c2l0ZQ%3d%3d
17. Cloud GL (1995) Optical Methods of Engineering Analysis, Cambridge University Press. https://doi.org/10.1017/CBO9780511575013

18. Ghiglia DC and Pritt MD (1998) Two-dimensional phase unwrapping: theory, algorithms, and software. Wiley. https://books.google.com/books/about/Two_dimensional_phase_unwrapping.html?id=pQtTAAAAMAAJ
19. Ding H (2003) Prediction and Validation of Thermomechanical Reliability in Electronic Packaging, Ph.D. Dissertation, School of Mechanical Engineering, Georgia Institute of Technology, Atlanta, GA. http://hdl.handle.net/1853/17565
20. Takeda M, Ina H, Kobayashi S (1982) Fourier-transform method of fringe-pattern analysis for computer-based topography and interferometry. J Opt Soc Am 72:156–160
21. Proll K-P, Nivet J-M, Körner K, Tiziani HJ (2003) Microscopic three-dimensional topometry with ferroelectric liquid-crystal-on-silicon displays. Appl Opt 42:1773–1778
22. Falcao G, Hurtos N, Massich J (2008) Plane-based calibration of a projectorcamera system. VIBOT Master 9(1):1-12. Available at https://www.researchgate.net/profile/Joan_Massich/publication/265230871_Planebased_calibration_of_a_projector-camera_system/links/54db26570cf261ce15cf4cd1/Plane-basedcalibration-of-a-projector-camera-system.pdf
23. Sukthankar R, Stockton RG, and Mullin MD (2001) Smarter presentations: exploiting homography in camera-projector systems, in Proceedings of IEEE International Conference on Computer Vision 482:247–253
24. Lohry WF, Xu Y, and Zhang S (2009) Optimal checkerboard selection for structured light system calibration, Optical Inspection and Metrology for Non-Optics Industries, vol. 7432. San Diego, CA, p 743202. https://doi.org/10.1117/12.823829
25. Kang S and Ume IC (2014) Automatic segmentation method for segmenting PBGA package and PWB regions during warpage measurement of unpainted PWB assembly, in International Symposium on Microelectronics, San Diego pp. 580–584
26. Solomon C and Breckon T (2011) Fundamentals of Digital Image Processing: A Practical Approach with Examples in Matlab. Wiley. https://doi.org/10.1002/9780470689776
27. Canny J (1986) A computational approach to edge detection. IEEE Trans Pattern Anal Mach Intell 8:679–698
28. Adams R, Bischof L (1994) Seeded region growing. IEEE Trans Pattern Anal Mach Intell 16:641–647
29. Zhucheng L (2010) Accurate calibration methods for small-depth objects in digital fringe projection, Ph.D. Dissertation, Dept. of Mechanical and Aerospace Engineering, Seoul National University, Seoul, South Korea. http://www.riss.kr/search/detail/DetailView.do?p_mat_type=be54d9b8bc7cdb09&control_no=3867b4d4d74c5425ffe0bdc3ef48d419
30. Harding K (2012) Handbook of optical dimensional metrology. CRC Press. https://www.crcpress.com/Handbook-of-Optical-Dimensional-Metrology/Harding/p/book/9781439854815
31. Pham H (2006) Springer handbook of engineering statistics. Springer. http://www.springer.com/us/book/9781852338060
32. Badiru AB, Agustiady T (2012) Statistical techniques for project control. CRC Press. https://www.crcpress.com/Statistical-Techniques-for-Project-Control/Badiru-Agustiady/p/book/9781420083170